Near-Field Inductive Coupling Induced Polarization Control in Metasurfaces

Cong, Longqing; Srivastava, Yogesh Kumar; Singh, Ranjan

2016

Cong, L., Srivastava, Y. K., & Singh, R. (2016). Near-Field Inductive Coupling Induced Polarization Control in Metasurfaces. Advanced Optical Materials, 4(6), 848-852.

https://hdl.handle.net/10356/83727

https://doi.org/10.1002/adom.201500681

DOI: 10.1002/((please add manuscript number))
Article type: Communication

Near-field inductive coupling induced polarization control in metasurfaces

*Longqing Cong, Yogesh Kumar Srivastava and Ranjan Singh**

Longqing Cong, Yogesh Kumar Srivastava, Prof. Ranjan Singh
Division of Physics and Applied Physics, School of Physical and Mathematical Sciences, Nanyang Technological University, Singapore 637371, Singapore
Centre for Disruptive Photonic Technologies, School of Physical and Mathematical Sciences, Nanyang Technological University, Singapore 637371, Singapore
E-mail: ranjans@ntu.edu.sg

Keywords: (polarization control, inductive coupling, terahertz, switchable coupling)

Abstract: Arbitrary manipulation of polarization of light has been an important research area that has applications in holography, vector beam generation, beam splitting, and design of wave plates. In this work, we investigate the near-field inductive coupling induced cross-polarized radiation in metasurfaces and its dominant role in polarization control. The inductive coupling in the chosen meta-molecular design depends on the mutual orientation of the meta-atoms that could tailor the coupling channel and thus the cross-polarized radiation is passively switched between “on” and “off” states leading to an effective control of the output polarization state of light. The non-intuitive tuning behavior of the inductively excited mode is interpreted through a circuit model where the exact location of the effective inductor in the meta-molecule dominates the coupling behavior. The switch on/off state of the coupling channel provides a new perspective of near-field coupling based passive and active control of polarization devices in applications such as holograms and encoded metamaterials.

Metamaterials provide a distinct platform to manipulate the electromagnetic properties of artificially designed media for active and passive device functionalities, such as cloaking,[1] sensing,[2] perfect absorption,[3] modulation[4] and negative refraction.[5, 6] Metasurfaces[7] are two-dimensional arrays of meta-film resonators that have critical dimensions much smaller than the operational wavelength. Split-ring resonators[8-11] (SRR) have been the most commonly used meta-atom unit cell design at the microwave and terahertz frequencies. However, different functionalities and spectral properties require varied designs that consists of in-plane coupled meta-atoms,[12-14] named as meta-molecule (MM) or the stacked layers of SRRs.[8]

Near-field coupling among the meta-atoms in a meta-molecule has recently been widely studied.[14,15] Dark modes have been used to achieve electromagnetically induced transparency,[16-18] however, their role in polarization conversion has not been investigated thoroughly. A detailed study of the intra coupling (via near fields between the meta-atoms) in a meta-molecule is based on the geometrical distance between the meta-atoms[19] and the study of polarization control effects originating from coupling has also been executed.[20] Arbitrary manipulation of local and global polarization of output radiation has been a very important research hot spot that finds application in holography,[21-23] beam splitter,[24] vector beam generation[25] and polarization control.[26-32] In this work, we provide a new perspective of near-field coupling where we demonstrate a passive switching of the near-field inductive coupling induced excitation in orthogonally twisted meta-atoms where the coupling channel is switched on in MM1 and switched off in MM2 within the same geometrical distance. The electromagnetic near-field coupling between the meta-atom induces the

cross-polarized radiation that is switched on and off when the coupling channel is switched on and off, which plays a dominant role in determining the output polarization state of light.

As shown in **Figure. 1**, we fabricated several planar meta-molecular arrays that consist of two orthogonal SRRs in each unit cell on a double-polished high resistivity silicon. The fabrication was performed using conventional photolithography, development, metallization and lift-off processes (See Experimental Section for detail). All the SRRs are identical in size that are made up of aluminum and the geometrical parameters are shown in Figure 1. The left and right SRRs in the meta-molecular unit cell are designated as SRR1 and SRR2, respectively. SRR1 and SRR2 are orthogonally twisted and the distance between them in the unit cell is constant at d = 3 μm to ensure that two SRRs are well within the near-field coupling distance.[19] The SRR2 in MM1 and MM2 are rotated clockwise and anticlockwise respectively by 90° relative to SRR1 in order to obtain the polarization dependent excitation of meta-atoms in the meta-molecule.

In order to measure the response of MM1 and MM2, we employed an 8-*f* antenna based terahertz time-domain spectroscopy (THz-TDS) system[33] with a set of polarizers inserted to coherently measure the co- and cross-polarized transmission signals (See Experimental Section for detail).[26] We obtained the time-domain waveforms and then converted them into frequency domain spectra with both amplitude and phase information using Fourier transformation. The transmission amplitude spectra $\left|\tilde{t}_{ji}(\omega)\right|$ and the phase information $\phi_{ji}(\omega)$ are obtained by $\tilde{t}_{ji}(\omega)=\tilde{t}_{ji}^{Sam}(\omega)/\tilde{t}_{ji}^{Ref}(\omega)$ where $\tilde{t}_{ji}^{Sam}(\omega)$ is the complex transmitted signal of metamaterial samples and $\tilde{t}_{ji}^{Ref}(\omega)$ is the complex transmitted reference signals, respectively. Here, the reference is an identical blank silicon substrate and i and j represent

the input and output polarization states. All the measurements were performed at normal incidence in dry nitrogen atmosphere. As shown in **Figures. 2(a)** and 2(b), we exhibit the co-polarized transmission spectra with *x*-polarized and *y*-polarized incidence, respectively. While comparing the response of MM1 and MM2 in Figure. 2(a) with *x*-polarized excitation where SRR1 is the directly excited meta-atom, a non-intuitive phenomenon occurs where MM1 and MM2 reveal disparate behaviors in the co-polarized spectra. The mode interference spectrum of MM1 is commonly known due to the inductive coupling between SRR1 and SRR2 where the directly excited SRR1 induces the resonance of the unexcited SRR2 through a magnetic dipole that is defined as indirectly excited meta-atom. Surprisingly, we do not observe any spectral splitting in MM2 which indicates the absence of inductive coupling between SRR1 and SRR2. A similar orientation dependent coupling behavior is also revealed in Figure. 2(b) with *y*-polarized incidence where SRR2 is directly excited. The spectra with *x*-polarized and *y*-polarized incidence reveal the different responses that originates from the anisotropy due to the rectangular unit cell design of the metamaterial lattice. The corresponding simulation spectra by using CST Microwave Studio in frequency domain solver with the same geometrical parameter and material properties as experiments (See Experimental Section) are exhibited in Figure. 2(c) and 2(d) that matched well with the measured data. The very fine details of the simulated spectra are not captured in experiments due to the limited resolution of the terahertz measurements. The response of an individual SRR array on an identical lattice where we excite the fundamental inductive-capacitive (LC) resonance is also simulated and shown as dash lines in the Figures 2(c) and (d) for reference in order to compare the eigen modes of individual SRR array to that of MM2. As we can observe, the spectra of MM2 almost match with

those of the corresponding individual SRR array, which demonstrates that the inductive coupling between the meta-atoms in MM2 disappears and the indirectly excited meta-atom is invisible in terms of the spectral signature.

To further understand the phenomenon of the orientation dependent inductive coupling, we measured as well as simulated the cross-polarized signals that is radiated from the indirectly excited SRR and thus is a measure of the coupling strength. In the orthogonally twisted SRR meta-molecule as shown in **Figure. 3(a)**, they would radiate the orthogonally polarized signals in the far field once both SRRs are directly and indirectly excited, which is demonstrated by the strong cross-polarized signal of MM1 in both measurement and simulation as shown in Figures. 3(b) and 3(c). However, the cross-polarized signal is extremely weak for MM2 as shown by the red curves in the same graph. The disagreement of the cross-polarized signal between the measurements and simulations originates from the limited scan time and extinction ratio of polarizers in the experiments, especially of the response of MM2 for which case the cross-polarized signal is extremely weak.

The orientation dependent near-field inductive coupling is visualized by the current distributions at 0.47 THz in Figures. 3(d) and 3(e), where SRR1 is directly excited with *x*-polarized illumination and SRR2 is the indirectly excited meta-atom whose eigen frequency of fundamental mode is also at 0.47 THz. In MM1, both SRRs upon excitation has surface current loops that form the magnetic dipoles due to bianisotropy[4, 9, 34] and thus the mode interference and the cross-polarized components are observed in the transmission spectra. In MM2, SRR1 shows directly excited surface current loop, whereas SRR2 does not show obvious surface current excitation neither by the external field nor by the near-field coupling from SRR1. Therefore, the neighboring meta-atom seems to have a minimal

interaction with the directly excited one, and thus the transmission spectra of MM2 appear to be similar to the intrinsic eigen mode LC resonance spectra of individual SRR array. This phenomenon is non-intuitive according to Faraday's law which states that the induced electromotive force (ε) in a circuit is proportional to the rate of change of the magnetic flux. Here in the two models of the SRR pair, the distance between the neighboring meta-atoms in one unit cell of MM1 and MM2 are kept identical to ensure that the same magnetic flux pierces through the indirectly excited SRRs. The intensity of the normalized far-field cross-polarized component is a measure of the induced electromotive force in the indirectly excited SRRs by inductive near-field coupling that is uncoupled from the incident light. The experimental and simulated results clearly show that the inductive coupling reveals completely different strength in these two cases.

We interpret the orientation dependent near-field coupling using a simple equivalent LC circuit model for the SRR as shown in Figures 3(d) and 3(e) where the split gap of the SRR is regarded as the effective capacitor (C) and the wire as the effective inductor (L) with the effective resistor (R) in the equivalent circuit model.[35,36] The relative positions of the effective inductor of the circuit model is important from the aspect of inductive coupling. The inductive coupling is through the effective inductor in the circuit and it is the distance between the neighboring inductor that determines strength of the near-field inductive coupling. Therefore, the coupling is much stronger in MM1 with the inductor distance being 3 μm than that in MM2 where the inductor is separated by 38 μm (See supporting information). Since the near-field inductive coupling strength has a strong signature in the far-field transmission spectra that depends on the far-field radiation from the orthogonally

coupled SRRs, the location of the capacitive gap in each SRR plays an important role in determining the overall transmitted spectral behavior (See supporting information).

In this near-field coupled system, there is a phase-lag of the radiation from the indirectly excited SRR that radiates the cross-polarized component as shown in the inset of **Figure. 4(a)** where the time-domain signal of the cross-polarized component shows the delay relative to the co-polarized component. With the delayed cross-polarized component radiating out to the far field, the polarization state of the output light is modulated by engineering the amplitude ratio and phase lag between the co- and the cross-polarized components.[8] In order to numerically describe the polarization states, we utilize Stokes parameters[29, 37] to describe the output states of the terahertz radiation as: $S_0 = \left|\tilde{t}_{xy}\right|^2 + \left|\tilde{t}_{yy}\right|^2$, $S_1 = \left|\tilde{t}_{xy}\right|^2 - \left|\tilde{t}_{yy}\right|^2$, $S_2 = 2\left|\tilde{t}_{xy}\right|\left|\tilde{t}_{yy}\right| cos\varphi_{del}$, and $S_3 = 2\left|\tilde{t}_{xy}\right|\left|\tilde{t}_{yy}\right| sin\varphi_{del}$, where φ_{del} is the phase difference ($\varphi_{del} = \varphi_{yy} - \varphi_{xy}$). By employing the Stokes parameters, we could calculate $tan2\psi = S_2/S_1$ and $sin2\chi = S_3/S_0$, where ψ and χ represent the angle of polarization ellipse (AOP) and ellipticity, respectively. The ellipticity $\chi = 45°$ indicates a perfect right-handed circularly polarized (RCP) light, and $\chi = -45°$ indicates a perfect left-handed circularly polarized (LCP) light, and $-45° < \chi < 45°$ represents elliptically (linearly, $\chi = 0°$) polarized light. We calculated the AOP as well as ellipticity of the output light with *y*-polarized incidence as shown in Figure 4. As shown in Figure. 4(a), the AOP is non-zero for MM1 with the polarization state being rotated by about -40° at 0.44 THz due to the existence of the strong cross-polarized component where ellipticity is 0°, however, the AOP of MM2 is nearly 0° due to the extremely weak cross-polarized component. Therefore, the output light is linearly polarized and rotated by -40° upon interaction with MM1 but

does not undergo any rotation while interacting with MM2 at 0.44 THz. Similarly in Figure. 4(b) that shows the ellipticity, there is a strong enhancement in MM1 reaching to -30° at 0.46 THz. This ellipticity originates from the phase lag of the cross-polarized component in MM1 while the ellipticity in MM2 is nearly absent without the cross-polarized component. The resultant polarization states at 0.46 THz are also shown as insets in Figure. 4 which clearly reveal the contrasting states with the change of orientation of indirectly excited SRR2 in MM1 and MM2. The large values of AOP and ellipticity highlights the potential of a simple near-field inductively coupled metasurface that could operate as a polarizer and a quarter wave plate with optimized structural parameters.

In summary, we have investigated the effect of inductive near-field coupling in orthogonally twisted SRR pairs which radiates the cross-polarized component in the far field. The coupling strength is measured through the amplitude of the cross-polarized component which radiates due to the near-field excitation of the inductively coupled orthogonally twisted SRR. In the two proposed configurations of MM1 and MM2 with the identical geometrical distance between the neighboring SRRs, the different coupling strength appears with different split-gap orientations of the indirectly excited SRR. This non-intuitive phenomenon is interpreted through the equivalent circuit model. With the phase lag of the cross-polarized component, the metasurface can function as a quarter wave plate device. The switch on/off behavior of the near-field coupling in the orthogonally twisted SRR meta-molecule can be applied for the active control of polarization states and polarization-division multiplexing devices in future terahertz and optical metamaterial technologies.

Methods

Simulations. The numerical simulations (transmission spectra and field distributions) were carried out using a commercially available software (CST Microwave Studio) by the finite-element frequency-domain solver with unit cell boundary conditions for each unit cell. The dimensions of each metasurface are specified in the main text and material properties are extracted from the experimental samples with the lossless silicon (ε = 11.78) and aluminum (σ = 3.72 × 10^7 S/m). The simulated transmission data was normalized in order to match the measured data.

Sample Fabrication. Conventional photolithography and thermal metallization process were employed to fabricate the samples. 200-nm-thick aluminum film was thermally evaporated on the patterned photoresist using a thermal evaporator. After the lift-off process in acetone, a pattern of concentric meta-molecule array was fabricated on top of a double polished high resistivity silicon substrate. All the samples studied in this work were fabricated on a 640 μm thick *n*-type silicon substrate through typical microelectronic fabrication procedure. The fabricated samples along with the optical microscope images are shown in Figure. 1.

Measurements. At normal incidence, the samples were characterized by THz-TDS system with three sets of wire-grid polarizers. The femtosecond fiber laser beam (90 *f*s, 60 mW at 1560 nm with 100 MHz repetition rate) was focused on a photo-conductive antenna to generate and detect the terahertz signals. To obtain the cross-polarized transmission signals, three sets of polarizers P1, P2 and P3 were inserted into the terahertz beam path between the transmitter and receiver. P1 was right after the transmitter to guarantee the linearly horizontal polarized incidence and P2 inserted after sample in order to filter the transmitted

co-polarized signal that was perpendicular to P1 and P3 were arranged 45° relative to P2, after which the transmitted signals can be detected by the receiver. For the co-polarized transmission of samples and the corresponding reference (dry nitrogen) signals, we rotated P2 by 90° and performed the measurement.

Supporting Information

Supporting Information is available from the Wiley Online Library or from the author.

Acknowledgements

L. C., Y. K. S. and R. S. acknowledge NTU startup Grant No. M4081282, MOE Tier 1 Grant No. M4011362 and MOE grant No. MOE2011-T3-1-005 for funding of this research.

Author contributions

L. C. and R. S. conceived the idea. L.C designed the experiments and performed all the measurements. Y. K. S. fabricated the samples. L. C. and R. S. discussed and analyzed the measured data. R. S. supervised the theory and the measurements. L. C. and R. S. prepared the manuscript.

Competing financial interests

The authors declare no competing financial interests.

References:

1. X. Ni, Z. J. Wong, M. Mrejen, Y. Wang and X. Zhang, *Science* **2015**, *349*, 1310.
2. L. Cong, S. Tan, R. Yahiaoui, F. Yan, W. Zhang and R. Singh, *Appl. Phys. Lett.* **2015**, *106*, 031107.
3. N. Landy, S. Sajuyigbe, J. Mock, D. Smith and W. Padilla, *Phys. Rev. Lett.* **2008**, *100*, 207402.
4. W. J. Padilla, A. J. Taylor, C. Highstrete, M. Lee and R. D. Averitt, *Phys. Rev. Lett.* **2006**, *96*, 107401.
5. J. Pendry, *Science* **2004**, *306*, 1353.
6. D. R. Smith, J. B. Pendry and M. C. Wiltshire, *Science* **2004**, *305*, 788.
7. N. Yu, P. Genevet, M. A. Kats, F. Aieta, J. P. Tetienne, F. Capasso and Z. Gaburro, *Science* **2011**, *334*, 333.
8. M. Decker, R. Zhao, C. Soukoulis, S. Linden and M. Wegener, *Opt. Lett.* **2010**, *35*, 1593.
9. T.-J. Yen, W. Padilla, N. Fang, D. Vier, D. Smith, J. Pendry, D. Basov and X. Zhang, *Science* **2004**, *303*, 1494.
10. R. Marqués, F. Mesa, J. Martel and F. Medina, *Antennas and Propagation, IEEE Transactions on* **2003**, *51*, 2572.
11. I. Sersic, M. Frimmer, E. Verhagen and A. F. Koenderink, *Phys. Rev. Lett.* **2009**, *103*, 213902.
12. N. Liu and H. Giessen, *Angew Chem Int Ed Engl* **2010**, *49*, 9838.
13. N. Liu, S. Kaiser and H. Giessen, *Adv. Mater.* **2008**, *20*, 4521.
14. N. Liu and H. Giessen, *Opt. Express* **2008**, *16*, 21233.
15. R. Singh, C. Rockstuhl, F. Lederer and W. Zhang, *Phys. Rev. B* **2009**, *79*, 085111.
16. Y. Guo, L. Yan, W. Pan, B. Luo, K. Wen, Z. Guo and X. Luo, *Opt. Express* **2012**, *20*, 24348.
17. P. Tassin, L. Zhang, T. Koschny, E. N. Economou and C. M. Soukoulis, *Phys. Rev. Lett.* **2009**, *102*, 053901.
18. S. Zhang, D. A. Genov, Y. Wang, M. Liu and X. Zhang, *Phys. Rev. Lett.* **2008**, *101*, 047401.
19. R. Singh, I. Al-Naib, D. R. Chowdhury, L. Cong, C. Rockstuhl and W. Zhang, *Appl. Phys. Lett.* **2014**, *105*, 081108.
20. B. Abasahl, S. Dutta-Gupta, C. Santschi and O. J. Martin, *Nano Lett.* **2013**, *13*, 4575.
21. D. Wen, F. Yue, G. Li, G. Zheng, K. Chan, S. Chen, M. Chen, K. F. Li, P. W. H. Wong and K. W. Cheah, *Nature Commun.* **2015**, *6*, 8241 (2015).
22. G. Zheng, H. Mühlenbernd, M. Kenney, G. Li, T. Zentgraf and S. Zhang, *Nature Nanotechnology* **2015**, *10*, 308.
23. L. Huang, X. Chen, H. Mühlenbernd, H. Zhang, S. Chen, B. Bai, Q. Tan, G. Jin, K.-W. Cheah and C.-W. Qiu, *Nature Commun.* **2013**, *4*, 2808.
24. M. Khorasaninejad, W. Zhu and K. Crozier, *Optica* **2015**, *2*, 376.
25. A. Arbabi, Y. Horie, M. Bagheri and A. Faraon, *Nature Nanotechnology* **2015**, *10*, 937.
26. L. Cong, N. Xu, W. Zhang and R. Singh, *Adv. Opt. Mater.* **2015**, *3*, 1176.
27. L. Cong, N. Xu, J. Han, W. Zhang and R. Singh, *Adv. Mater.* **2015**, *27*, 6630.

28. H. Cheng, S. Chen, P. Yu, J. Li, L. Deng and J. Tian, *Opt. Lett.* **2013**, *38*, 1567.
29. H. Cheng, S. Chen, P. Yu, J. Li, B. Xie, Z. Li and J. Tian, *Appl. Phys. Lett.* **2013**, *103*, 223102.
30. W. Liu, S. Chen, Z. Li, H. Cheng, P. Yu, J. Li and J. Tian, *Opt. Lett.* **2015**, *40*, 3185.
31. H. Cheng, Z. Liu, S. Chen and J. Tian, *Adv. Mater.* **2015**, *27*, 5410.
32. J. Li, P. Yu, H. Cheng, W. Liu, Z. Li, B. Xie, S. Chen and J. Tian, *Adv. Opt. Mater.* 2015, DOI: 10.1002/adom.201500398.
33. D. Grischkowsky, S. Keiding, M. v. Exter and C. Fattinger, *J. Opt. Soc. Am. B* **1990**, *7*, 2006.
34. H. Tao, A. Strikwerda, K. Fan, W. Padilla, X. Zhang and R. Averitt, *Phys. Rev. Lett.* **2009**, *103*, 147401.
35. X. Zhang, Q. Li, W. Cao, W. Yue, J. Gu, Z. Tian, J. Han and W. Zhang, *Chinese Opt. Lett.* **2011**, *9*, 110012.
36. J. D. Baena, J. Bonache, F. Martín, R. M. Sillero, F. Falcone, F. F. T. Lopetegi, M. A. Laso, J. G. García, I. Gil and M. F. Portillo, *Microwave Theory and Techniques, IEEE Transactions on* **2005**, *53*, 1451.
37. D. Goldstein and D. H. Goldstein, *Polarized Light, revised and expanded*. (CRC Press, 2011).

Figure Captions

Figure 1 | Experimental design and images of the fabricated samples. Images of (a) MM1 array (inductive coupling "on") and (b) MM2 (inductive coupling "off"). The inset shows the metamaterial unit cell which is composed of two identical SRRs. In MM1, SRR2 is rotated clockwise by 90° relative to SRR1 and in MM2, SRR2 rotated anticlockwise by 90° relative to SRR1.

Figure 2 | The measured and simulated amplitude transmission spectra. The co-polarized transmission spectra for (a) *x*-polarized and (b) *y*-polarized incidence in MM1 and MM2, respectively. (c) and (d) the corresponding simulated transmission spectra for the MM1, MM2 and individual SRR array.

Figure 3 | The cross-polarized amplitude transmission and surface currents distributions. (a) Schematic diagram of the MM array to induce the co- and cross-polarized radiation. (b) Measured and (c) simulated cross-polarized amplitude transmission for MM1 and MM2. The surface current distributions with *x*-polarized incidence for (d) MM1 and (e) MM2 and the corresponding effective circuit models.

Figure 4 | The calculated rotation angle and elliticity of the output radiation with *y*-polarized incidence. (a) The rotation angle of output polarization ellipse (inset: the time-

domain signals of co- and cross-polarized components); (b) The ellipticity of output polarization ellipse (inset: the output polarization states at 0.46 THz).

Figure. 1

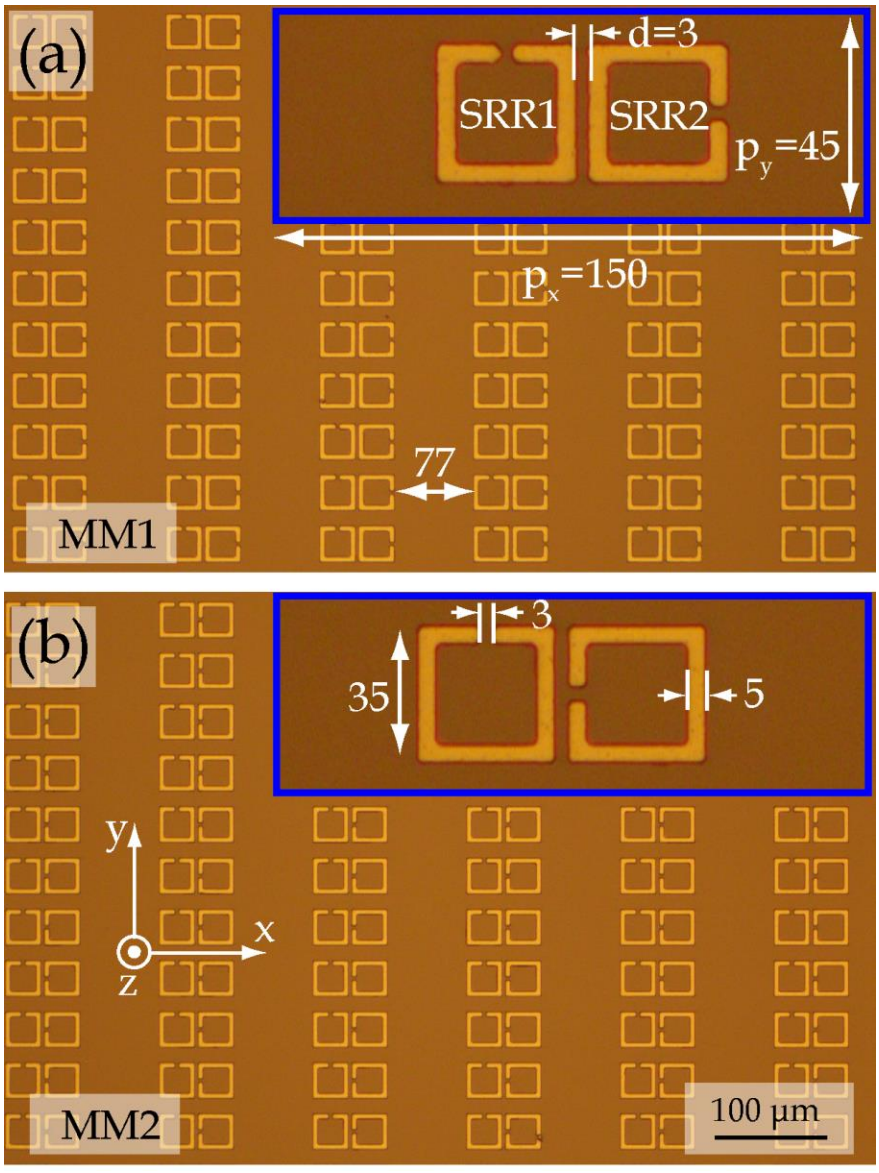

Figure. 2

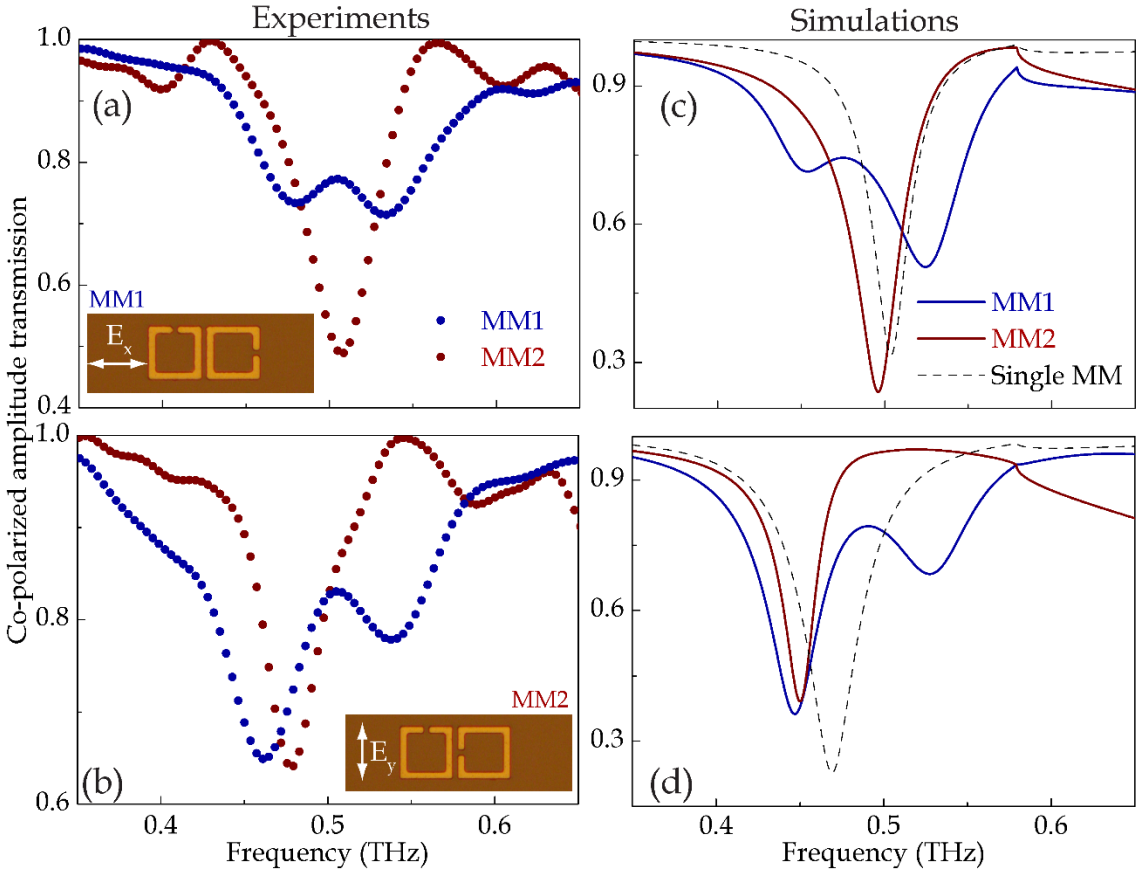
Experiments
Simulations
(a)
(b)
(c)
(d)
MM1
MM2
Single MM
E_x
E_y
Co-polarized amplitude transmission
Frequency (THz)
1.0
0.8
0.6
0.4
0.9
0.6
0.3
0.4
0.5
0.6

Figure. 3

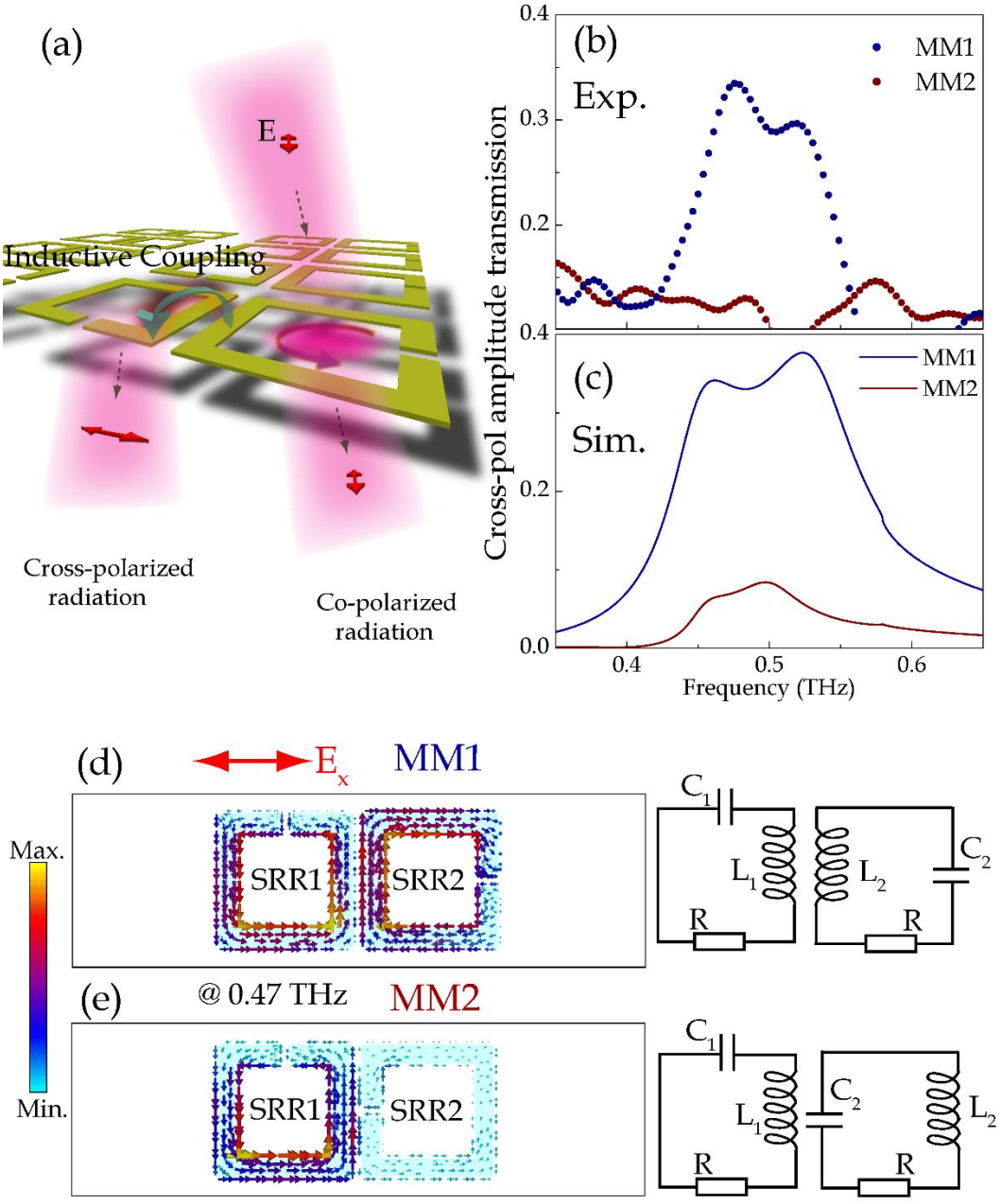
(a)
E
Inductive Coupling
Cross-polarized radiation
Co-polarized radiation
(b)
Exp.
MM1
MM2
(c)
Sim.
MM1
MM2
Cross-pol amplitude transmission
0.0
0.2
0.4
0.3
0.4
0.5
0.6
Frequency (THz)
(d)
E_x
MM1
SRR1
SRR2
C1
L1
R
L2
C2
R
Max.
Min.
(e)
@ 0.47 THz
MM2
SRR1
SRR2
C1
L1
R
C2
L2
R

Figure. 4

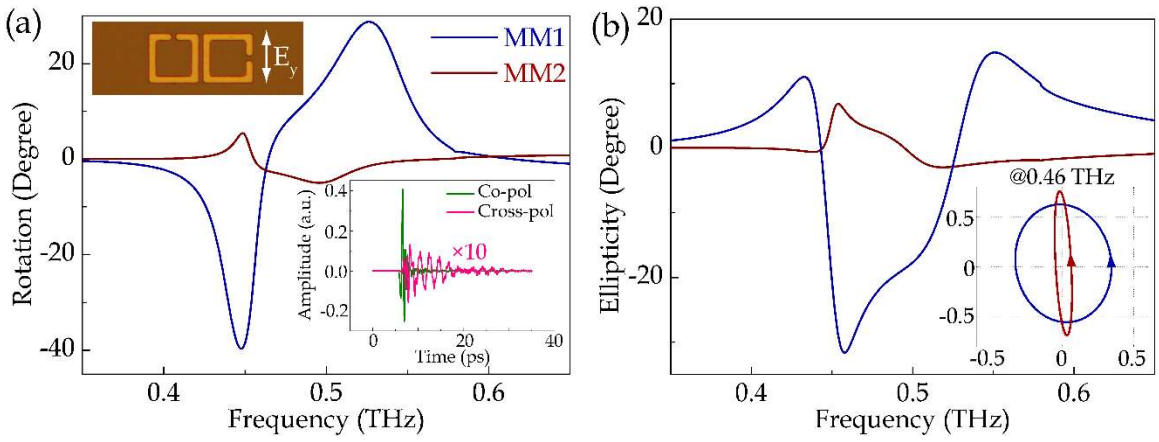
(a)
E_y
MM1
MM2
Rotation (Degree)
20
0
-20
-40
0.4
0.5
0.6
Frequency (THz)
Co-pol
Cross-pol
×10
Amplitude (a.u.)
0.4
0.2
0.0
-0.2
0
20
40
Time (ps)
(b)
Ellipticity (Degree)
20
0
-20
@0.46 THz
0.5
0
-0.5
-0.5
0
0.5
0.4
0.5
0.6
Frequency (THz)

Table of Content

The inductive coupling of the identical bianisotropic meta-atoms has been demonstrated to be dependent on the spatial distance. Here, we experimentally study a non-intuitive orientation dependent switchable coupling phenomenon and show the applications in polarization control of the proposed metasurface.

Keywords: (polarization control, inductive coupling, terahertz, switchable coupling)

Longqing Cong, Yogesh Kumar Srivastava and Ranjan Singh*

Near-field inductive coupling induced polarization control in metasurfaces

ToC figure

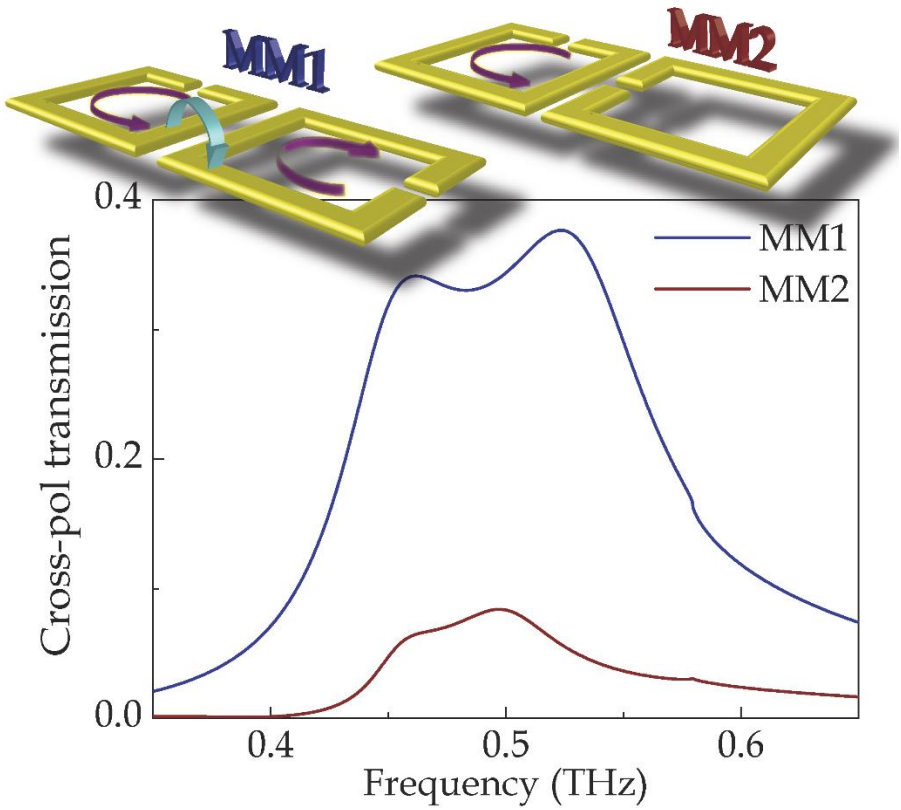

Supporting Information

Near-field inductive coupling induced polarization control in metasurfaces

*Longqing Cong, Yogesh Kumar Srivastava and Ranjan Singh**

S1. Demonstration of equivalent circuit model

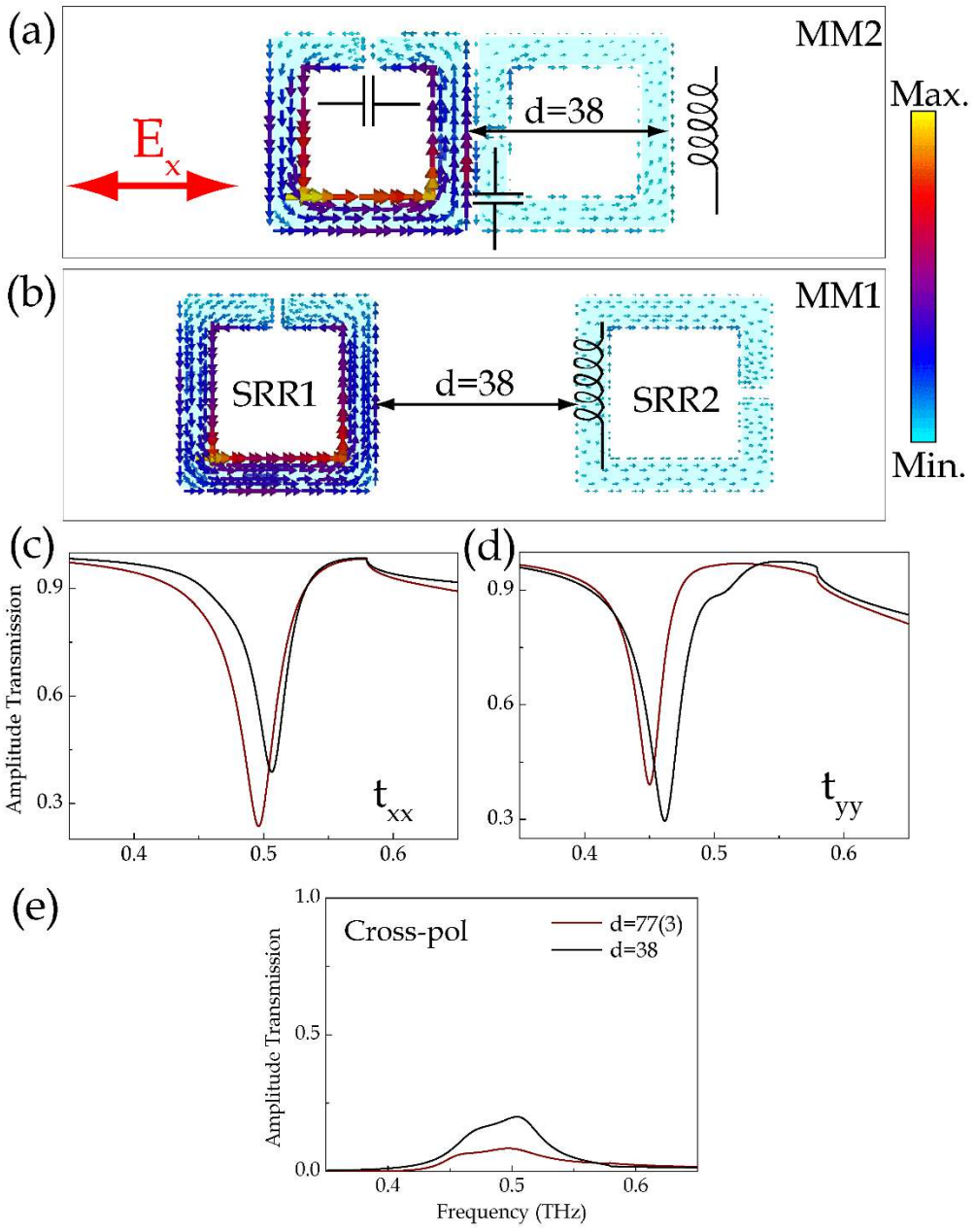

Figure S1 | Demonstration of equivalent circuit model. The surface current distributions in the case of (a) MM2 with distance between meta-atoms at 3 μm and (b) MM1 model with distance at 38 μm. The simulated co-polarized transmission spectra for the two cases with (c) *x*-polarized and (d) *y*-polarized incidence and (e) the cross-polarized transmission spectra.

To demonstrate the validity of the proposed equivalent circuit model for the interpretation of the non-intuitive inductive coupling behaviors, we performed detail simulations as shown in Figure S1. In the proposed meta-molecular array, the period of the unit cell along *x* and *y* axes are 45 and 150 μm, respectively. With the size of the SRR being 35 μm, the distance d = 3 μm in MM2 is equivalent to the case of d = 77 μm in MM1. From this point of view, it could be obvious that the inductive coupling would not be strong in MM2 as per the large geometrical distance. However, the near-field inductive coupling between the neighboring unit cell would be dominate at the case of d = 77 μm in MM1.

The equivalent circuit model explains the non-intuitive phenomenon based on the location of the effective inductor in the coupled circuit. Besides considering the effective values of the inductor to calculate the eigen resonance frequency of SRR by employing the equivalent circuit model, the position of the inductor and capacitor is also important in a coupled meta-molecular system. In the proposed double SRR system, the inductive coupling is considered through the effective inductor and thus the location of the inductor plays an important role in determining the near-field coupling behavior. In MM2, the equivalent distance between the neighboring inductor is about 38 μm and we compare the surface current distributions as well as the transmission spectra of MM1 with d = 38 μm and MM2 with d = 3 μm as shown in **Figure S1**. From Figures. S1(a) and (b), the surface

current distributions reveal similar behavior where SRR1 is the directly excited meta-atom and the indirectly excited SRR2 is extremely weak due to the weak inductive coupling at large geometrical separation. A more accurate comparison is observed from the co- and cross-polarized transmission spectra as shown in Figures. S1(c)-(e), where we could observe the difference between these two cases. The strength of inductive coupling is slightly stronger in case of MM1 than that in case of MM2 in the cross-polarized transmission spectra. The slight difference originates from the location of the capacitive gap in each SRR that is discussed in part S3. In MM1, the inductive coupling is direct from SRR1 to SRR2 whereas there is an effective capacitor between the two coupled inductors in MM2 that inhibits the strong inductive coupling.

S2. The near-field coupling effect on the efficiency of the cross-polarized transmission

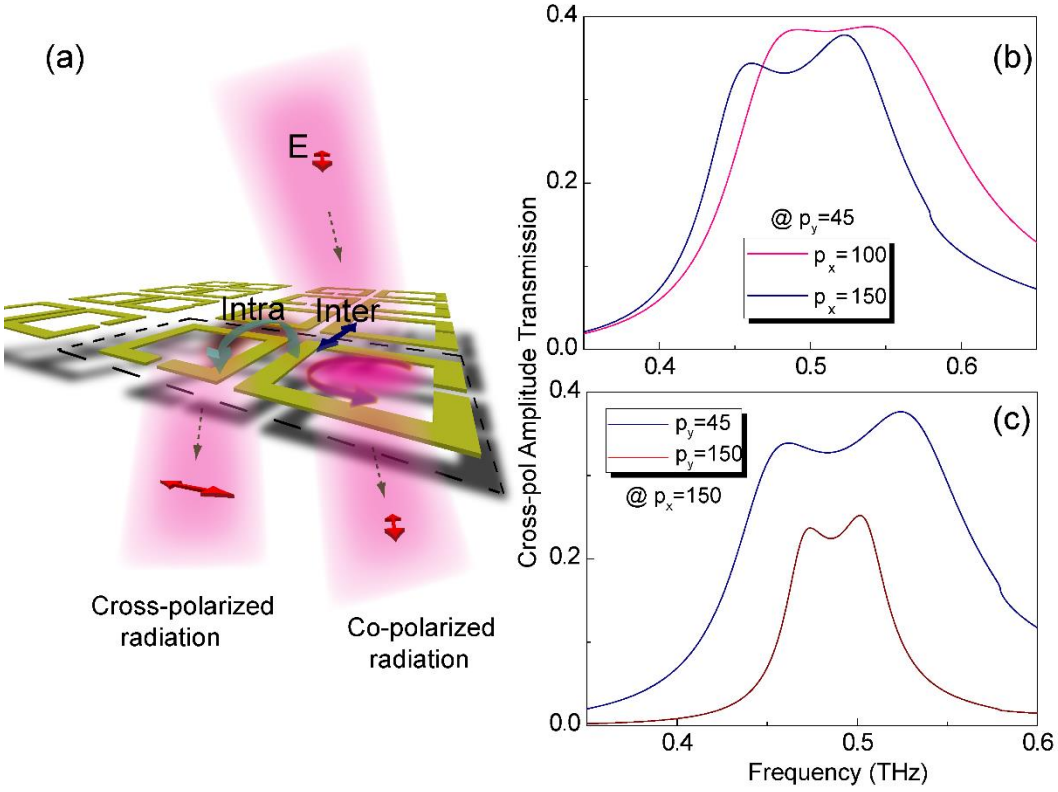

Figure S2 | Effects of coupling led enhancement of the cross-polarized component. (a) The schematic diagram of intra meta-atom coupling and inter unit cell coupling. (b) The inter unit cell coupling spectra along *x*-axis with *y*-axis periodicity fixed at 45 μm. (c) The inter unit cell coupling spectra along *y*-axis with *x*-axis periodicity fixed at 150 μm.

In the case for MM1 as shown in **Figure S2(a)**, the intra coupling between the adjacent meta-atoms in a unit cell dominates the inductive coupling strength and the inter unit cell coupling between SRR2 and SRR1 of the right-hand side unit cell is negligible due to the large values of p_x. However, this effect would not be negligible if p_x is small enough so that the inter coupling strength gets enhanced. Therefore, the cross-polarized component will be enhanced. As shown in Figure. S2(b), the cross-polarized transmission amplitude grows when the periodicity along *x*-axis (p_x) is adjusted from p_x = 150 μm to p_x = 100 μm with constant p_y = 45 μm. However, there is extremely weak enhancement by adjusting inter coupling distance along the *x*-axis since the inductive coupling is prohibited between SRR2 and SRR1 in the right-hand side unit cell as we have discussed in the main text. For comparison, we also show the amplitude enhancement effects of the inter coupling along *y*-axis as shown in Figure. S2(c) where p_x is fixed at 150 μm and p_y is varied from p_y = 150 μm to p_y = 45 μm. It clearly shows that the cross-polarized amplitude is enhanced strongly along with a significant broadening of the operation bandwidth.

S3. Detailed discussion of the capacitive (electric) and the inductive (magnetic) coupling

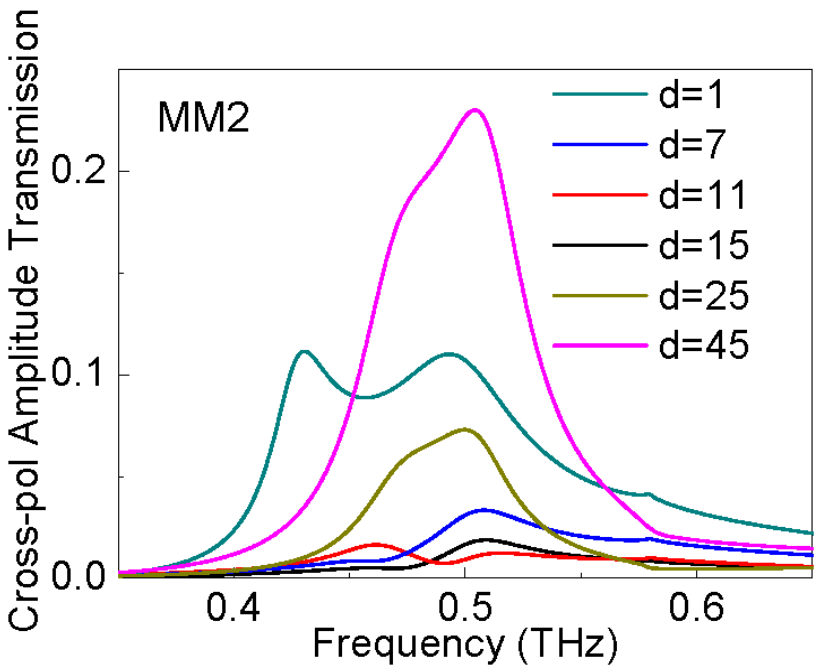

Figure S3 | The simulated cross-polarized transmission spectra of MM2 at d = 1 μm, 7 μm, 11 μm, 15 μm, 25 μm, and 45 μm, respectively.

In order to interpret the near-field coupling phenomenon in detail, we investigate the transmission spectra of MM2 at different coupling distance "*d*" as shown in Figure S3. As discussed in the main text, the cross-polarized transmission spectra directly indicates the coupling strength and thus we show the cross-polarized transmission spectra of MM2. We have discussed that MM1 reveals a much stronger coupling strength than MM2 and it is the location of effective inductor in the equivalent circuit model that determines the coupling strength. To further confirm this, we exhibit the evolution of the cross-polarized transmission spectra of MM2 in Figure S3. We can clearly observe the change in the amplitude which varies from strong to weak and then becomes strong again as distance d was varied from 1 μm to 45 μm. According to the inductive coupling mechanism, the

coupling from the directly excited SRR to indirectly excited SRR is through an effective inductor that mainly depends on the distance *d* between the two inductors. However, the indirectly excited SRR radiates the cross-polarized component from the orthogonal capacitive gap which also depends on the distance *d*. As known from previous works, the smaller the distance *d* is, the larger is the inductive coupling.[1] However, the cross-polarized radiation is suppressed when the gap of the indirectly excited SRR2 is close to the wire of the neighbour SRR1 according to the transmission spectra in Figure S3, which also explains the phenomenon in Figure S1(e). The cross-polarized amplitude varies from large to small when *d* varies from 1 μm to 11 μm. The suppression of the cross-polarized transmitted radiation due to competing capacitive (electric) and the inductive (magnetic) coupling occurs at around *d* = 15 μm. As the distance in MM2 becomes larger, the indirectly excited SRR2 becomes closer to the SRR1 of the neighbouring unit cell which becomes similar to the case of MM1 and thus the cross-polarized radiation is not suppressed since the capacitive gap remains far away from the effective inductor. Therefore, the cross-polarized amplitude is proportional to the distance *d* that determines the inductive coupling strength.

References:

1. R. Singh, I. Al-Naib, D. R. Chowdhury, L. Cong, C. Rockstuhl and W. Zhang, *Appl. Phys. Lett*. **2014**, *105*, 081108.